A wideband two-way UHF stripline combiner

M. Abdolhamidi[1], M. Mohammad-Taheri[2], and M. Ahmadi Ali-Abad[3].

Receireceived:2016-01-24 Accepted:2016-08-19

Abstract

A two-way combiner with a built-in broadside-coupled stripline coupler, for digital video broadcast transmitters at UHF frequencies is presented. The combiner exhibits more than 28dB of return losses at all ports in the entire digital television broadcast frequency band (namely 470MHz-862MHz). The isolation levels between each pair of isolated ports are more than 29dB in the above frequency band. The excellent frequency responses are obtained due to our modifications in the structure of the constituent coupled-line coupler in the form of the utilization of a multi-section broadside-coupled stripline structure and the elimination of the improper stripline bends. While the presented combiner satisfies all standard industrial requirements such as 3U (three Rack Units) distance of input ports, it shows wideband and non-resonant behavior in the frequency responses. In addition, by introducing a novel asymmetry in the structure of the intrinsic coupled-line coupler, significant reductions in the combiner size and cost are achieved.

***Index Terms*— Directional coupler, High power, Compact and low cost structure.**

I. INTRODUCTION

WITH the introduction of the directional couplers, these structures are widely explored and used by the RF and microwave engineering researchers [1], [2]. Coupled-line directional couplers are of the most common and commercial types of directional couplers which are mainly designed in the form of either the edge-coupled coupler [3] or the broadside (stacked)–coupled coupler [4]. In the recent scientific reports, both of these architectures have been widely implemented for the design and development of wideband directional couplers [5], couplers with novel and specific topologies [6], and directional couplers for specific applications such as impedance transformers [7]. However, the realization of directional couplers for high power industrial applications, are rarely addressed [8]. In this paper, the design and fabrication of a 2-way high power combiner for the efficient combination of two high power digital video broadcast signals at UHF frequencies is introduced. This combiner has an enhanced built-in broadside-coupled coupled-line coupler. An external view of the combiner is shown in Fig. 1 (a). In this combiner, the input ports are high power standard 1 5/8” female coaxial connectors with hot-plug connection capability, while the output port and the absorber load port are 1 5/8” male connectors. The input ports are excited by two equal-amplitude but quadrature in phase high power UHF signals. The constructive summation of two equal amplitude and quadrature in phase signals is available at the output port. However, that of the destructive summation will be transmitted to the absorber load. All building components including the multi-step coupling structure and other fixing components are placed in the main metallic box. The designed configuration of the combiner has created prominent UHF responses. These responses include scattering

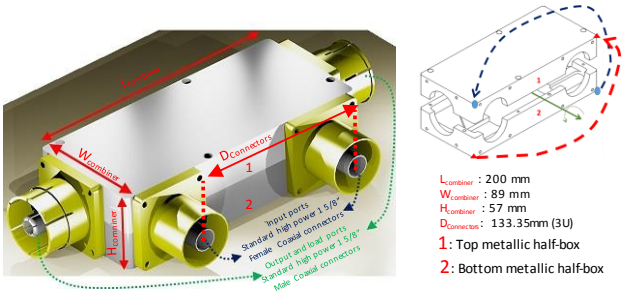

(a) (b)

Fig .1: Architecture of the combiner: (a) external perspective view and building elements. (b) Uniqueness of two half-boxes comprising the main body of the combiner.

[1]PhD student of Electrical Engineering-Telecommunications, Department of Electrical and Computer Engineering, Faculty of Engineering, Tehran University e-mail: abdolhamidi@ut.ac.ir

[2]Associate Professor, Department of Electrical and Computer Engineering, Faculty of Engineering, Tehran University

[3] Member of the Board and CEO Frafrnd, Pvt. e-mail: ahmadi@fara-afrand.com

parameters and power handling capability. More detailed explanations of the design and frequency responses of the combiner are described in the following sections.

II. DESIGN DESCRIPTION

The presented combiner is designed and fabricated in a shielded stripline (SSL) -based architecture. The shielded stripline waveguide, as shown in Fig. 2-a, comprises a metallic strip which is floated in a dielectric medium and surrounded by a metallic shielding. Some of the properties of this structure such as the simple fabrication process and the ability to transmit single-mode TEM waves, tailors it for high power sub-gigahertz applications. The electromagnetic (EM) wave carried by this waveguide can be coupled to another SSL in a coupled-line configuration whose cross section is shown in Fig. 2-b. It can be seen that the structure consists of two opposite-face parallel strips. The overall configuration is usually called the broadside-coupled stripline (SBCSL). It has two dominant TEM guiding modes, namely the common and he differential modes. The E-field distributions of these

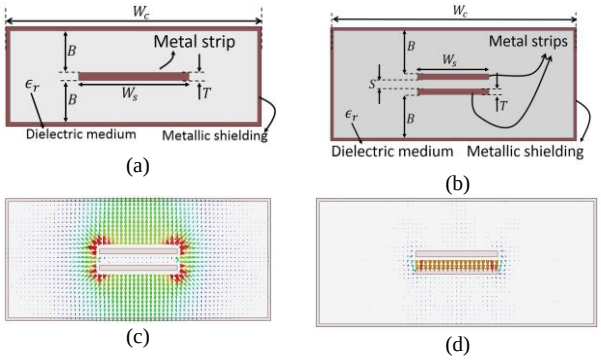

Fig .2: Shielded stripline waveguiding structures and E-field distributions: (a) SSL. (b) SBCSL. (c) common mode E-field distribution in SBCSL. (d) differential mode E-field distribution in SBCSL.

modes are illustrated in Figs. 2-c, d, respectively. The fundamental part of our proposed combiner is a piece of the SBCSL. We want to design a two-way combiner in the range of 470 ~ 862 MHz with the center frequency of 666 MHz. We start our design with a piece of the SBCSL whose length is equal to the quarter wavelength at 666 MHz. Fig. 3 shows the 3D structure of the SBCSL section besides its equivalent circuit model. The full-wave simulations and the circuit model analysis are carried out in Ansoft-HFSS and ADS-Schematics, respectively. Three characteristic values, namely the odd and the even impedances and the electrical length are enough to define the presented ideal model. The odd and the even impedances in the ideal model correspond to the differential mode and the common mode characteristic impedance in the full-wave simulations, respectively. There is a one to one correspondence between the illustrated ports of the model and the lumped ports of the full-wave simulations. It can be shown [9] that if one of the ports (1 to 4) are excited by an incoming wave from a $Z_0\,(ohm)$-source and all other ports are connected to $Z_0\,(ohm)$ terminations, the power reflection at the excited port vanishes if

$$\sqrt{Z_{0_{even}} \times Z_{0_{odd}}} = Z_0 \qquad (1)$$

We set the odd and the even impedances to hold (1). Now, if we suppose that the incoming waves from the equal-amplitude and quadrature in phase ports 1 and 2 are constructively combined in port 3, the structure of Fig. 3 will approximately be a 3dB coupler. By a simple model optimization, we find that as a 3dB combiner/splitter, the frequency response of the model in the mentioned frequency band is optimized if we

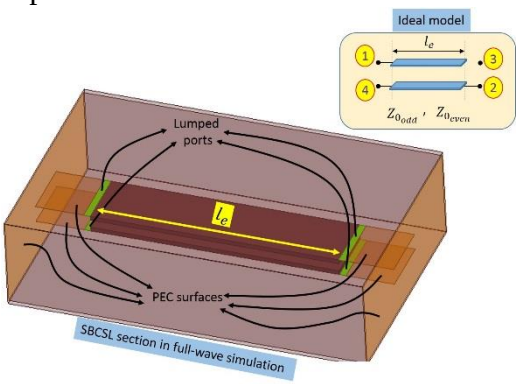

Fig .3: A piece of a SBCSL and its simple model.

choose $Z_{0_{even}} \approx 125.5\ \Omega$,$Z_{0_{odd}} \approx 19.9\ \Omega$ and $l_e = \left(\frac{\lambda_g}{4}\right)$ $@666\ MHz$. The scattering parameters of the model with these characteristic values calculated at $Z_0 = 50\ \Omega$ ports are shown in Fig. 4-a. It is inferred from the figure that the levels of the power

reflections are extremely low and the difference between the direct transmission level ($|S_{31}|$) and the coupled transmission level ($|S_{32}|$) in the entire frequency band is less than or equal to 0.5dB. However, the full-wave simulation results are not comparably outstanding. The additional required boundary conditions and the inserted lumped-port excitations contribute to some unwanted errors in the simulations. The scattering parameters of the SBCSL section based on the EM simulation is shown in Fig. 4-b. The results show that the return losses at the ports and the difference between the direct-transmission level and the coupled transmission level have been increased. In addition, the frequency response is taken under a frequency shift because of the fringing fields at the strips ends. However, the EM simulation will have more accurate results if the excitation ports become TEM wave-ports. The dimensions of the simulated SBCSL section are listed in Table 1 which are according to the definitions depicted in Fig.2-b.

Now, we want to use this SBCSL section as a building block of our combiner. The position of the input and the output ports of our combiner has been previously illustrated in

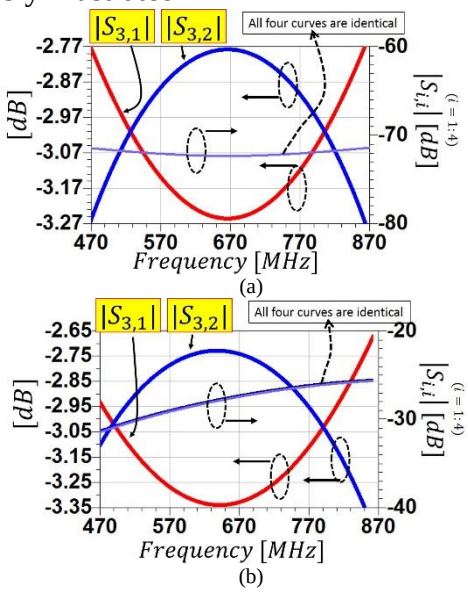

Fig .4: The scattering parameters of a quarter wavelength SBCSL section as shown in Fig. 3: (a) ideal model, (b) full-wave analysis.

Table 1: Dimensions of the SBCSL section.

W_s	T	S	B	W_c	L_e	ϵ_r
26.6 mm	2 mm	3.7 mm	16.15 mm	90 mm	112.5 mm	1 (air)

Fig. 1-a. That figure shows that the input ports are located at a sidewall and the output port and the load port are located at two other opposite sidewalls. It means that we need two stripline bends (Fig. 5) at both ends of the SBCSL section to properly connect our input coaxial ports. As shown in Fig. 5, after this modification, the combiner will consist of a basic SBCSL section, two 90-deg SSL bends, and four connecting 50 Ω SSL sections. The figure shows that the longitudinal distance of the inserted metered bends is kept at 112.5 mm ($\frac{\lambda_g}{4}$ @ 666 MHz). The scattering parameters of the structure are plotted in Fig. 6. As can be seen, the inserted bends significantly affect the performance of the combiner in terms of its couplings, isolations and return losses at the ports. In addition to the decrease in the power coupling level, the return losses and the isolation level of the input ports ($-|S_{21}|$) are both deteriorated. The reason for this unwanted degradation of responses lies in the fact that the connecting SSL sections which are shown in Fig. 5 are not isolated and decoupled from each other; but actually they form a coupled stripline structure whose odd and even impedances are varying values. It means that the metered bends and the connecting strips are also contributing to the proportion of the coupled power (power transmitted from port 2 to port 3). Fig. 7 explicitly shows this fact. This figure shows the E-field intensity distribution between two strips at 666 MHz when an incoming TEM wave excites port 1 and all other ports are connected to the 50 Ω terminations. The figure implies that the E-field intensity is

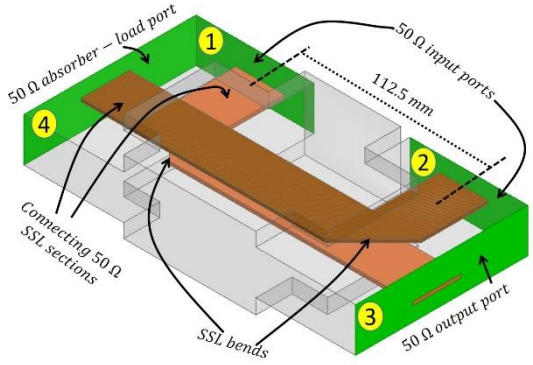

Fig .5: Basic structure of the SBCSL combiner.

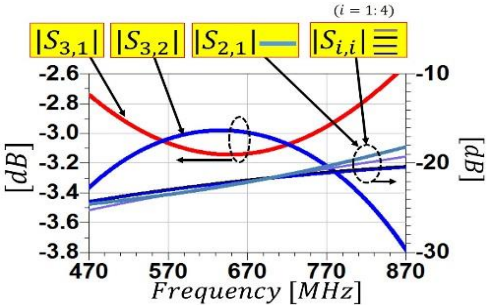

Fig .6: Frequency response of the combiner shown in Fig. 5

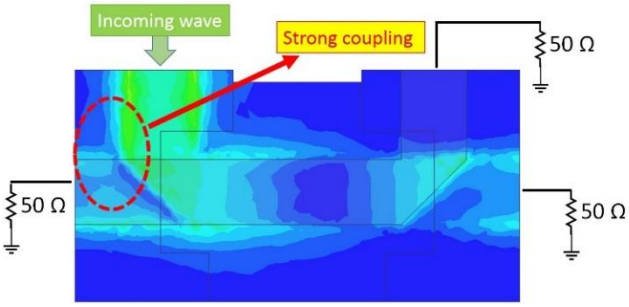

Fig .7: E-field intensity distribution between two strips.

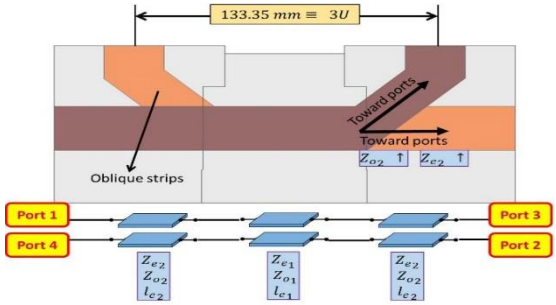

Fig .8: The structure of the combiner for 3U standard and its circuit model.

considerable around the metered bend and in the vicinity of the connecting strips. So, we should take into account these contributions in our design procedure.

To simplify the procedure and to suppress the modelling of the metered bend, firstly, we replace the metered bends and the connecting strips by two oblique strips (Fig. 8). This replacement will help us to provide the required 3U distance between the input ports, as well (each rack unit (U) equals 1.75 inch). Fig.8 also contains a simple equivalent circuit of the structure, where the SBCSL section is modeled by a non-quarter wavelength pair of coupled lines and the loosely-coupled connecting strips are modeled by a pair of couple lines whose odd and even impedances are varying. Because of the higher level of the mutual coupling, the closer parts of the connecting strips to the SBCSL section have lower odd and even impedances than the farther parts. Thus, in the depicted circuit model Z_{e_2} and Z_{o_2} should be varying values. This will create difficulties in the modeling of the structure. Instead, we can use multi-section connecting strips having smaller lengths. Each of these sections can be approximately modeled by a coupled-line transmission line having fixed odd and even impedances.

The approximate circuit model of our proposed two-way combiner is shown in Fig. 9-a. The figure shows that the combiner simply consists of seven coupled-line sections and four connecting SSL sections. Each couple-lines section is realized in the form of an SBCSL section. The combiner has a symmetrical configuration. The overall structure of the circuit model in addition to the values of the odd and even impedances are all chosen according

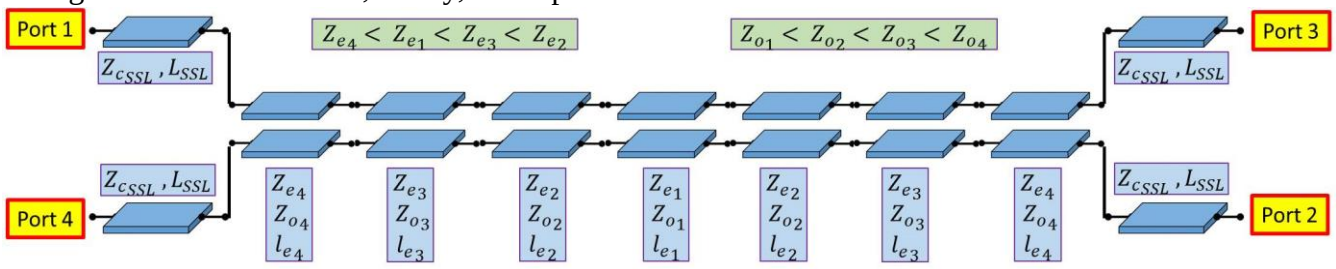

Fig .9: An optimized implementation of the primary design

Z_{e_1}	Z_{o_1}	l_{e_1}	Z_{e_2}	Z_{o_2}	l_{e_2}	Z_{e_3}	Z_{o_3}	l_{e_3}	Z_{e_4}	Z_{o_4}	l_{e_4}	$Z_{C_{SSL}}$	$L_{C_{SSL}}$
105 Ω	14 Ω	26 deg	165 Ω	25 Ω	16.5 deg	150 Ω	32 Ω	9 deg	62 Ω	37 Ω	20 deg	80 Ω	10 deg

Table 2: Optimized values of the circuit model of Fig. 9.

to an optimization on the scattering parameters of the combiner. The optimization process has three goals, namely reducing the level of the return losses at the ports, increasing the isolation level of the input ports and reducing the difference of the direct transmission level ($|S_{31}|$) and the coupled transmission level ($|S_{32}|$) in the entire frequency band. The optimized values for the circuit of Fig. 9 are listed in Table 2. The scattering parameters of this circuit with optimized values of Table 2 is shown in Fig. 10. The figure shows that the return losses at all ports and the isolation level of the input port are both better than 33 dB in the entire frequency band. In addition, the difference between the coupled transmission level and the direct transmission level is less than 0.5dB in the entire band. These scattering parameters are highly similar to the parameters achieved for the ideal one-section coupler of Fig. 3 whose simulation results were depicted in Fig. 4-a. It means that by the proper replacement of the 90-deg stripline bends and the connecting strips by the multi-section coupled-line structure we have achieved nearly ideal scattering parameters for our combiner. The next step will be the realization of the circuit of Fig. 9 in an SBCSL architecture.

Fig. 11 shows the structure of the realized two-way combiner based on the circuit model of Fig. 9.

Because of its symmetric structure, the descriptions are shown for only one half of the combiner. The figure shows that the low-impedance SBCSL section and the high-impedance SBCSL section both have fixed odd and even impedance values. But, the high-odd impedance section and the low-even impedance section have varying impedances. Thus, we design these latter

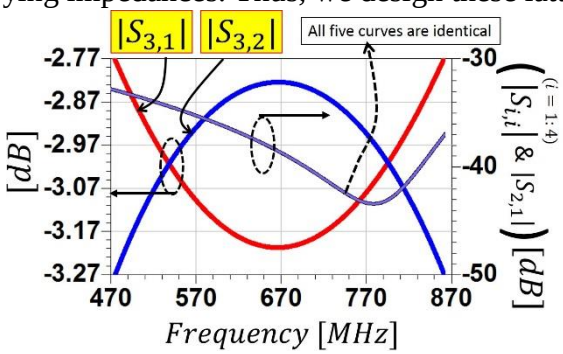

Fig .10: Scattering parameters of the circuit shown in Fig. 9.

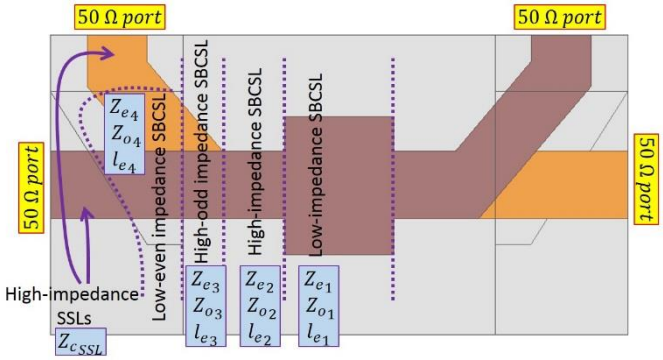

Fig .11: SBCSL realization of the circuit model of Fig. 10.

sections in a way that the average values of their odd and even impedances be equal to the optimized values presented in Table 2. The scattering parameters of this combiner is shown in Fig. 12. As can be seen, the full-wave simulation results are slightly different from those of the circuit model simulation. The return losses at the ports and the isolation level of the input ports are better than 27 dB and 30 dB in the entire frequency band, respectively. More, the difference between the direct transmission level and coupled transmission level have been increased to a maximum of 1 dB. These results show that the combiner needs a fine finishing optimization before the fabrication. In addition, we need to take into account some limitations put by the fabrication processes on the mechanical structure of the combiner. We have considered all these limitations in our final simulations. Some of the brilliant mechanical properties of the fabricated combiner besides the final enhancements made on it are presented in the next section.

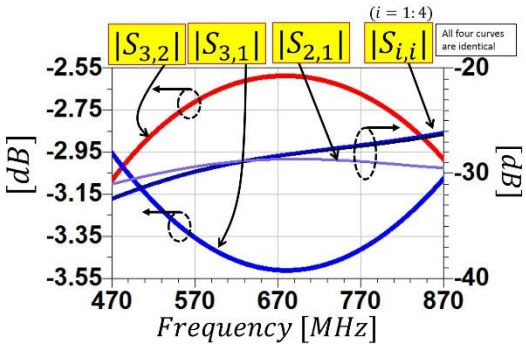

Fig .12: Scattering parameters of the structure of Fig. 11.

III. Fabrication and Measurement

For the ease of mass production and cost efficiency, the main metallic body of the combiner is fabricated in the form of two identical half-

boxes. The uniqueness of two half-boxes comprising the main body of the combiner was previously shown in Fig. 1 (b). As can be seen from that figure, if the bottom half-box is rotated around the shown axis and the specified corners are drawn to their new positions, this half-box is converted to the top half-box. The center-to-center distance of the input coaxial ports is 133.35mm (3U), and the length, width and height of the box are 200mm, 89mm and 57mm respectively. An interior view of the final combiner is pictured in Fig. 13. The figure implies that in addition to the previously explained parts, the combiner has high power standard coaxial connectors and some PTFE supports. In this figure the top half-box is removed for a better illustration. The metallic body is made from aluminum to minimize the construction cost while the strips are made from copper to reduce the ohmic losses. The depicted PTFE supports, firmly fix the gap distance between two strips and the distances of the strips to the metallic walls. The input signals fed by coaxial connectors are transmitted through stripline sections and combined at the high power output port.

A closer view of the low impedance SBCSL section and the high impedance SBCSL section is shown in Fig. 14. The introduction of the shown asymmetry has notably reduced the combiner width ($W_{combiner}$ in Fig. 1 (a)). Fig. 14 shows that the present location of the sidewall in the asymmetric structure is 17mm away from its previous location in the symmetric structure. It means that the reduced volume is 194cm^3 corresponding to $17mm \times 200mm \times 57mm$. The scattering parameters degradation due to the metallic wall displacement is thoroughly compensated by a further fine tuning. A photo of the measurement setup is shown in Fig15. The

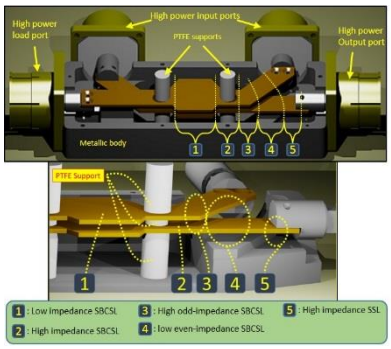

Fig. 13: Internal view of the fabricated combiner.

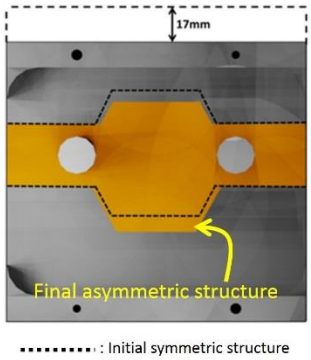

Fig .14: A closer view of the asymmetrical SBCSL section.

measurement is performed with an 8753C hp vector network analyzer using 1 5/8”-to-n transformers which are attached to all ports. These transformers enable one to make the measurement with n-type coaxial cables. The figure shows an arrangement for the measurement of the input to output transmission. For this measurement, the next input and the absorber load ports are connected to 50Ohm terminations. Figs. 16 (a)-(d) show the measured and simulated scattering parameters of the fabricated combiner. The simulation results are those of a full-wave simulation on the optimized structure in Ansoft HFSS software. It should be noted that our desired frequency band is still 470MHz-862MHz which is the assigned band for the terrestrial digital video broadcasting. In these figures, ports 1, 2, 3, and 4 are two input ports, the output port and the absorbing load port, respectively.

As can be seen from Fig. 16(a), the return losses are better than 28dB at all ports and have smooth and non-resonant behaviors in the entire frequency band. Fig. 16(b) shows that the isolations are better than 29dB in the same frequency band.

Phase quadrature property is clearly shown in Fig. 16(c) in the entire frequency band. Fig. 16(d) shows that the couplings from the input ports to the output port are -3.05dB $\pm 0.3dB$ in the entire frequency band which is very close to the ideal value of $-3\ dB\ \pm 0.25\ dB$. The measurements and the final full-wave simulations are in good agreements and the overall loss of the combiner is less than 0.05dB.

We have tested the combiner with two 750Watt COFDM DVB-T input signals. With 0.05dB of the insertion loss, about 10Watts of UHF power is

dissipated in the combiner which does not make any major problem in the long-term performance of the combiner.

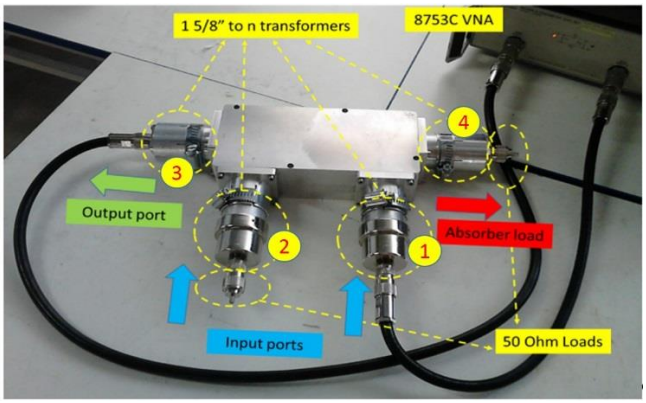

Fig .15: Measurement setup of the fabricated two-way combiner.

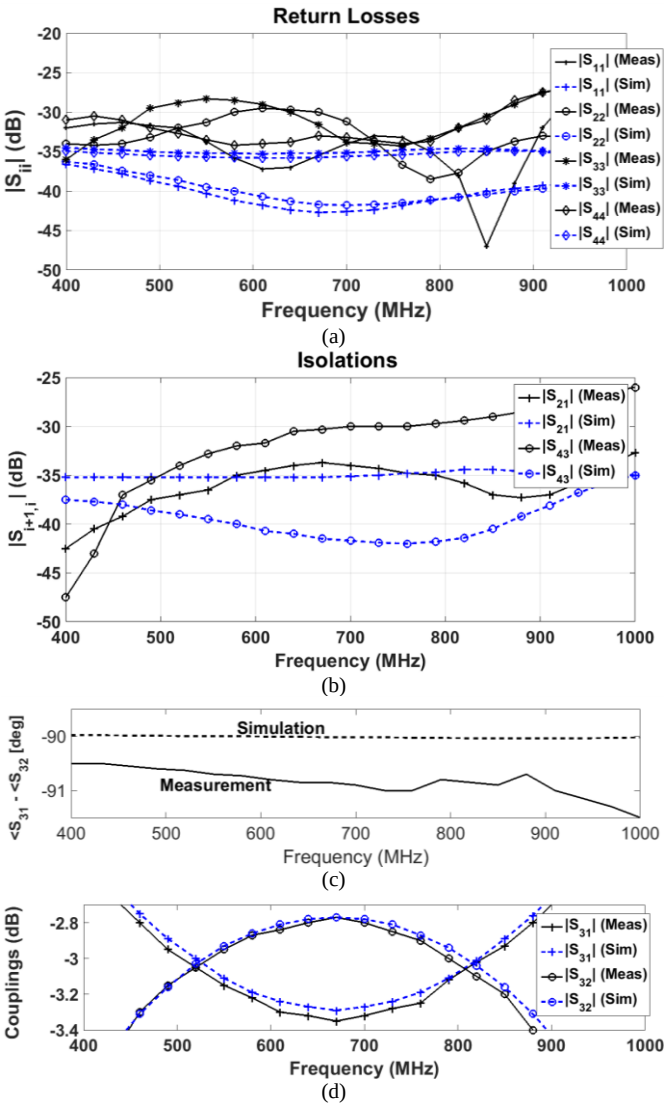

Fig. 16: Measurement results.

IV. Conclusion

In this paper, we designed and fabricated a high power combiner which is used for terrestrial video broadcasting. We have improved the combiner performance by making some modifications in the well-known structure of the built-in broadside-coupled stripline directional coupler. In addition, we inserted the multi-section matching circuits to our designed combiner to achieve wide-band performances. The fabricated combiner has shown acceptable performances for both small and high power exciting signals.

Acknowledgment

The authors would like to thank Mr. Ezzati of FaraAfrand Co. for his collaboration in the mechanical assembly and RF measurements.

References

[1] S. B. Cohn, and R. Levy, "History of microwave passive components with particular attention to directional couplers," *IEEE Trans. Microw. Theory Tech.* vol. 32, no. 9, pp. *1046-1054*, Sep. 1984.

[2] P. Meyer, J. C. Kruger, "Wideband crossed guide waveguide directional couplers", Microwave Symposium Digest, 1998 IEEE MTT-S International, vol. 1, 253-256, June 1998.

[3] J. Muller, et al, "Directional coupler compensation with optimally positioned capacitors", *IEEE Trans. Microw. Theory Tech*. vol. 59, no. 11, pp. 2824-2832, Sep. 2011.

[4] G. Ryu, et al, "A novel 3-dB coupler for MMIC using air-gap stacked microstrip lines", *IEEE Microw. Wireless Compon. Lett.*, vol. 10, no. 1, pp. 1-3, Jan. 2000.

[5] Hee-Ran Ahn, S. Nam, "Wideband microstrip coupled-line ring hybrids for high power division ratios", *IEEE Trans. Microw. Theory Tech*. vol. 61, no. 5, pp. 1768-1780, May 2013.

[6] K. Staszek, et al., "Multisection couplers with coupled-line sections having unequal lengths", *IEEE Trans. Microw. Theory Tech*. vol. 62, no. 7, pp. 1461-1469, July 2014.

[7] Hee-Ran Ahn, K. Bumman, "Transmission-line directional couplers for impedance transforming", *IEEE Microw. Wireless Compon. Lett.*, vol. 16, no. 10, pp. 537-539, Oct. 2006.

[8] V. Teppati, et al., "Broad-band coaxial directional couplers for high-power applications", *IEEE Trans.*

Microw. Theory Tech. vol. 51, no. 3, pp. 994-997, Apr. 2003.

[9] Design equations for broadside and edgewise stripline couplers, Rogers Cor., Az. USA [Online]. Available: https://www.rogerscorp.com/documents/781/acs/Design-Equations-for-Broadside-and-Edgewise-Stripline.pdf.